

Chapter 1

TileCal: The Hadronic Section of the Central ATLAS Calorimeter

K. Anderson², T. Del Prete⁴, E. Fullana¹, J. Huston³, C. Roda⁴ and R. Stanek¹

¹ *High Energy Physics Division, Argonne National Laboratory, Argonne,
IL 60439, USA*

² *University of Chicago, Chicago, Illinois, USA*

³ *Michigan State University, East Lansing, Michigan, USA*

⁴ *Pisa University and INFN, Pisa, Italy*

This section describes the concepts behind TileCal design, the requirements and the constraints that have finally produced ATLAS central hadronic calorimeter (*from Nino*).

1.1. TileCal design: motivation and requirements

The central hadronic calorimeter of ATLAS (the Tile Calorimeter, also known as TileCal) is a sampling calorimeter with steel as absorber and scintillating tiles as active medium. The calorimeter has been described in detail previously in several papers; here, we describe primarily the manner in which we arrived at the final Tilecal design.

In 1991,¹ it was known that the calorimeter resolution in a sampling hadronic calorimeter is not critically dependent on the orientation of the active medium. The understanding was that, at the end of a hadronic shower, low energy charged particles had velocities nearly isotropically distributed, as in a gas. Thus, a non-standard orientation of the active medium could be exploited in order to optimize hermeticity, while maintaining a relatively good energy resolution. Scintillating tiles, for example, could be oriented inside a steel absorber in the $r - \phi$ plane (see Fig.1.3), i.e. parallel to the direction of the incoming particles. The readout can then be performed via wavelength shifting (WLS) fibers coupled to the radial edges of the scintillator plates. Fibers could be routed in the radial direction, fitting in small slots in the absorber. This configuration is illustrated in Fig. 1.1. At a radius outside the absorber, the fibers could easily be grouped in order to obtain the needed calorimeter segmentation, and then coupled to photomultiplier tubes (PMTs).

At rapidities close to zero the scintillating tiles are nearly parallel to the primary particles. Thus the percentage of active material crossed by collimated showers depends strongly on the impact point. However TileCal is placed downstream of

2 *K. Anderson², T. Del Prete⁴, E. Fullana¹, J. Huston³, C. Roda⁴ and R. Stanek¹*

an electromagnetic calorimeter, most of the particles from the interaction will have already started to shower, and thus any channelling effect will be limited. To prevent the particles from traversing too long of a path inside the active material, the scintillator tiles can be made small and staggered with respect to each other.

This concept was validated and refined in detailed analyses of data acquired with prototype modules at test beams.^{2,3}

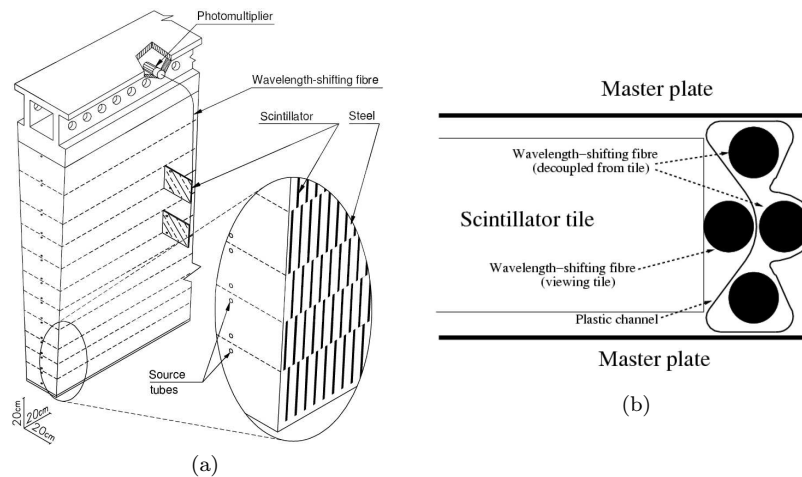


Fig. 1.1. (a) A schematic showing the sampling structure of the tile calorimeter and the integration of scintillator tiles and readout fibers with the absorber structure running radially from the interaction point. (b) A radial view schematic of the integration between the absorber structure, scintillator tiles and the fibers.

Other conceptual designs had also been considered as possibilities for the central ATLAS hadron calorimeter. For example, a design using a lead-liquid argon calorimeter (10 cm Pb plates and 4 mm Ar) was simulated in Monte Carlo. The resulting performance was found to not be superior to the Tilecal design. Similar conclusions were reached for a lead-scintillating tile geometry.¹

In addition, prototypes of an integrated electromagnetic-hadronic calorimeter using lead and scintillating fibers (“SPACAL”) were also built and tested.⁴ This option was seriously considered for the complete calorimeter system but was finally rejected for preference to a better performance electromagnetic section (now liquid argon) and a less expensive hadronic section.

Ultimately it was decided that the Tilecal option for the hadron calorimeter, complemented by a lead/liquid argon calorimeter (LAr) for the electromagnetic section, not only could achieve the physics goals but was also more modular and cost-effective.

The overall TileCal geometry was, in part, determined by the surrounding detectors: the liquid argon electromagnetic calorimeter inside and the muon spectrometer outside. The total thickness of the calorimeter system is a minimum of 10 inter-

action lengths (λ). Simulation studies indicate that a thickness of 9λ provides sufficient containment of the hadronic cascades for precision measurements both of jet properties and E_{miss}^T .

Another essential constraint was that the construction of TileCal was modular so that institutions around the globe could contribute with their resources, expertise and personnel to cut down the overall cost and the time needed to complete the work. TileCal elements were assembled in several laboratories in Russia, in the Czech Republic, Italy, Spain and the USA. The raw materials and finished elements were shipped back and forth across the globe over a four year time period. In spite of the apparent disjoint effort the strict tolerances required for the mechanical construction (about $100 \mu\text{m}$) were maintained in all the modules and the tight time schedule was fulfilled to within few weeks. The mechanical assembly details are discussed in Sec. 1.2.1.

In parallel with the design and construction of the mechanical components, *R&D* projects to optimize the optics were started. Since commercial tiles are both expensive and produced at a low rate an alternative technique of scintillator production was developed based on injection molding⁵⁻⁷. This method proved both cost and time effective with a drawback of a lower light budget. The light budget was recovered by optimizing the light transmission to the photo-multipliers: high quality optical fibers and efficient tile-fiber-PMT coupling.⁸⁻¹⁰ Details of all the optics aspects are discussed in section 1.2.5.

It was demonstrated in the very first prototype modules that the TileCal design was capable of producing a light yield of more than 50 photoelectrons per GeV of energy deposited in the absorber.

1.2. Tilecal solutions

1.2.1. *Mechanics*

The Tile calorimeter¹¹ for ATLAS^{12,13} is physically the largest component in this system with the function of extending the depth of calorimetry to wholly contain hadronic showers from pp collisions at the interaction point.

The TileCal scintillators are located in pockets in the steel structure and read out using wavelength-shifting fibers coupled to photo-multipliers located inside the outer support girders of the calorimeter structure.

In addition to its role as a detector for high energy particles, the Tile calorimeter provides the direct support of the liquid argon electromagnetic calorimeter in the barrel region, and of the liquid argon electromagnetic and hadronic calorimeters in the endcap region. Through these, it indirectly supports the inner tracking system and the beam pipe. The steel absorber, and in particular the support girders, provides the flux return for the solenoidal field from the central tracker solenoid.

Finally, the end surfaces of the barrel calorimeter are used to mount services, power supplies and readout crates for the inner tracking systems and for the elec-

4 *K. Anderson², T. Del Prete⁴, E. Fullana¹, J. Huston³, C. Roda⁴ and R. Stanek¹*

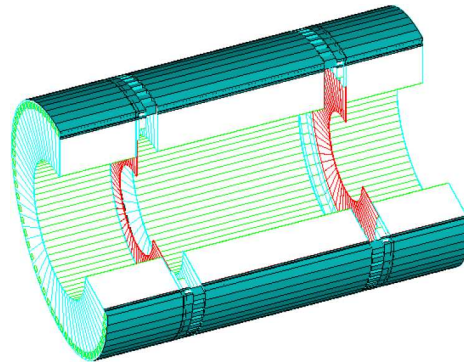


Fig. 1.2. The Tile calorimeter system in the ATLAS experiment at the Large Hadron Collider.

tromagnetic calorimeter section.

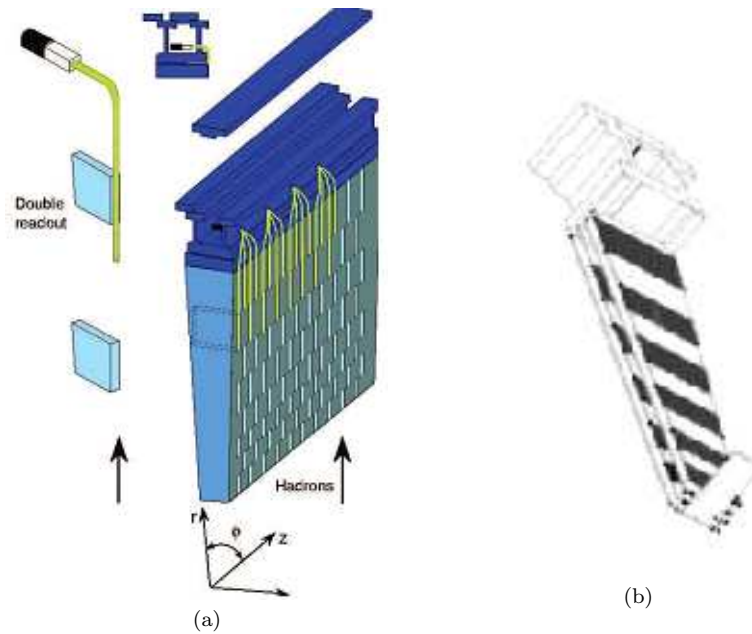


Fig. 1.3. (a) The Tile Calorimeter module design with the placement of all the optics elements (tiles, fibers and phototubes). Double Readout refers to the fact that both edges of the tiles are readout into separate phototubes. (b) The right-hand sketch shows the periodicity of the steel absorber as discussed below.

1.2.2. *The Principles of the Detector Design*

Some of the considerations in the development of the design of the TileCal can be summarized with the following statements:

- the overall cost should be minimized;
- good hermeticity;
- good energy linearity and resolution;
- modularity for parallel construction at several participating institutions;
- implement the flux return for the central solenoid and shielding for the front end electronics.

The Tile calorimeter is constructed in 3 sections, one central barrel and two extended barrels, each section comprising 64 individually constructed modules, which are stacked on each other to form each cylinder (Fig. 1.2). The central barrel covers the rapidity region $|\eta| < 1.7$ while the extended barrels have coverage of $1.4 < |\eta| < 3.2$. A barrel module weighs 20020 kg and an extended barrel module weighs 9600 kg. The mechanical structure has a nominal outer diameter of 4230 mm and an inner diameter of 2288 mm. A barrel (extended barrel) module has a length of 5640 mm (2900 mm). The calorimeter itself is self-supporting and rests simply on support saddles placed in the lower regions of the structure. The instrumented region of the calorimeter has a radial length of 1.64 m, and contributes 7.4λ for particles emitted at 90 degrees to the interaction point.

1.2.3. *Module Construction*

Each of the 256 modules is constructed in the following fashion. The absorber structure is formed using steel laminations, and has the unique feature that the steel plates run radially outward from the beam axis. This is the feature of the mechanical design which allows the fiducial acceptance of this calorimeter to be maximized. A schematic of the calorimeter structure is shown in Figs.1.3 and 1.1. The structure is a glued and welded steel lamination of full-length 5mm thick trapezoidal plates (master plates) spanning the full radial dimension of the module, and smaller 4 mm thick trapezoidal plates (spacer plates) interspersed along their length to form pockets in which the scintillator tiles are inserted. The spacer plates are set back from the edge of the master plate outer envelope by approximately 1.5 mm to provide a slot in which the readout fibers are inserted. The scintillator tiles are inserted into the gaps between the spacer plates resulting in an iron to scintillator ratio of 4.67:1 by volume. In addition, the plates have 22 precisely located holes through which the tubes for the Cs system (see section ??) calibration are inserted along the entire length of the structure.

In order to facilitate a relatively straight-forward construction procedure for precision modules, the absorber structure for each of the modules is first fabricated into submodules, which then are stacked and welded along the length of a support

6 *K. Anderson², T. Del Prete⁴, E. Fullana¹, J. Huston³, C. Roda⁴ and R. Stanek¹*

girder to form each module. This is illustrated in Fig. 1.4a.

1.2.4. Submodule Construction and Module Production

Eight standard submodules and two customized submodules are used to construct an extended barrel module, while eighteen standard submodules and one customized submodule are used to construct a barrel module. Die stamping was used to produce the master and spacer plates, again to realize the precision needed for the module envelope and for cost-effective production¹⁴. A nearly finished extended barrel module is shown in Fig.1.4b.

The girder is the outer structural support of the module. In addition to providing the outer bearing surface, the support girder provides the largest magnetic flux return for the central solenoid and also serves as a convenient location for the phototubes and front-end readout electronics. Low voltage power supplies, cooling and readout cables enter at the end of each of the girders. These are all contained in extensions of the girder called fingers, which provide shielding from the return magnetic field as well as physical protection for cables and connectors.

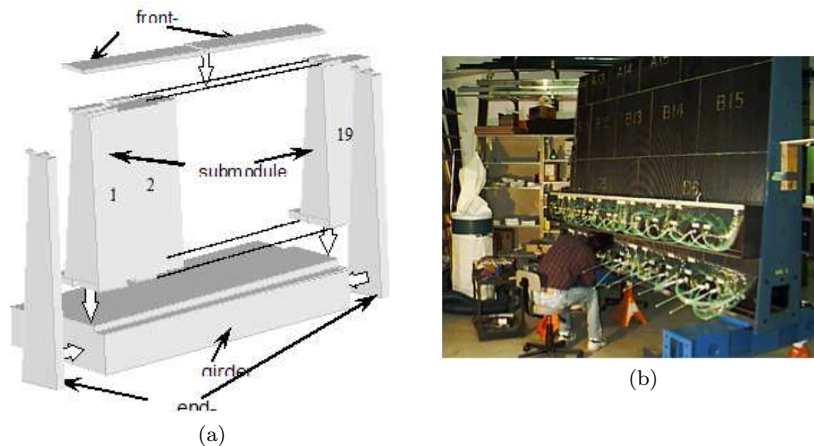


Fig. 1.4. (a) A sketch of the assembly of submodules on the girder forming a module. (b) On the right is shown a partially completed extended barrel module with details of the fiber routing clearly seen.

In the region between the barrel and extended barrel calorimeters, the services to the inner detector systems and the LAr cryostat flange result in dead material. In order to help correct for the energy loss in this material, an Intermediate Tile Calorimeter (ITC) and scintillators are installed in this region. This is illustrated in Fig. 1.5.

Due to the wedge shape nature of the modules, and designing for a self-supporting structure, the calorimeters were constructed by stacking each module on

Intermediate Tile Calorimeter Concept

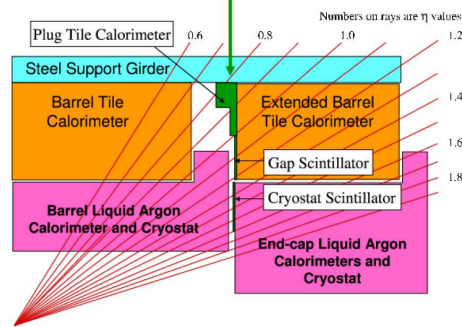


Fig. 1.5. A cut through the calorimeter system at the interface between barrel and extended barrel calorimeter.

top of the previous one, with appropriate shimming at the inner and outer radius to ensure closure at the top with the last module. The installation of the ATLAS detector in the experimental cavern was started in 2004. The three TileCal barrels were first pre-assembled on the surface. This allowed a check that the strict geometrical constraints, a few millimeters over a few meters, were fulfilled, and that the design for the complicated integration of cable services could be successfully implemented. The experience gained in the pre-assembly phase permitted a solution of many installation problems before facing the assembly in the experimental cavern. The TileCal was then partially dismantled to be lowered into the experimental cavern. The assembly in the cavern was completed in December 2005 and the TileCal was the first ATLAS sub-detector to provide cosmic muon data.

1.2.5. Optics

The driving concept behind the optics is to achieve and maintain a uniform, minimum light yield, such that the detector resolution is not compromised by lack of photo-statistics or by non-uniformities. Key to the physics performance of the TileCal is the optical budget; through the chain from scintillator to PMT, we require that a minimum ionizing particle (MIP) produces at least 0.5 photo-electrons (PE). This response leads to 20 photo-electrons produced per GeV deposited in the calorimeter. The contribution from photo-statistics is small relative to the intrinsic resolution endemic to hadron calorimeters. Based on past experiences with similar calorimeter systems, we expect an average 1-3% loss in light per year. A safety factor of 2 was added, leading to the requirement of at least 1 PE per MIP.

A non-uniformity of tile response can also degrade the physics performance of TileCal. Due to the large transverse size of hadron showers and the sharing of energy between the electromagnetic and hadronic sections of the ATLAS calorimetry, the non-uniformity requirements for the TileCal are less stringent than for the LAr calorimeter. Monte Carlo simulations show that a non-uniformity of 10% rms would

result in an increase of the constant term of the calorimeter resolution of 1%. To realize this 10% goal, it is necessary to restrict the non-uniformity within a tile, tile-to-tile fluctuations and fiber-to-fiber fluctuations each below 5%.⁷

The mechanical structure and the scintillator orientation of the TileCal necessitates the use of a very large number of scintillating tiles, of the order of 460,000, with 11 different radial sizes (59 tons of scintillator). Each of the scintillating tiles has a thickness of 3 mm. The standard technology for production of highest quality plastic scintillator uses styrene polymerization between two high quality glass plates. This process is slow and relatively expensive since large pieces of scintillator are cast and then are cut into the shapes required and subsequently polished.

The light budget adopted for the TileCal allows for the use of tiles produced by injection molding. Tiles produced by such a process typically have a lower light yield than cast scintillator. The injection molding process uses commercially available optically transparent granulated polystyrene pellets mixed with a primary and secondary scintillating dye (PTP and POPOP) adjusted to optimize the light yield and uniformity. As mentioned previously, there are 11 different radial sizes for the tile, but only 4 different tile widths. Thus, it was possible to produce the 11 different types of tiles using only 4 different molds with removable inserts, further reducing the cost and complexity. The mold surfaces were machined very smooth, so no additional polishing step for the tiles was required.

The surface of each tile is quite sensitive to scratching and crazing, so it was necessary to protect each tile. Welded Tyvek© sleeves were developed, into which each tile was inserted after fabrication. The reflectivity of the Tyvek resulted in an increase in the tile light yield of approximately 20%. An increase in the light yield at the ends of the tiles precluded the uniformity within a tile as discussed above. Thus, masking for the Tyvek sleeves was introduced. The masks are printed on the Tyvek material prior to the production of the sleeves and reduced any non-uniformity of response across the tile to less than 5%.

The blue scintillation light from the tiles is collected by wavelength-shifting (WLS) fibers coupled to the ϕ edges of the tiles, as shown in Fig.1.3. The mechanical and optical requirements are satisfied by the use of 1 mm diameter, double-clad polystyrene optical fibers, produced by Kuraray (Y11(200)MS). The double layer of cladding not only increases the light yield of the fibers but adds to their durability. A fast (< 10 ns) wavelength-shifting dye in the fiber shifts the scintillator light to wavelengths of 490 nm, providing a long attenuation length for transmission through the fibers, as well as matching to the response of the photo-cathodes in the PMTs. In order to improve the light yield and uniformity, the ends of the WLS fibers are polished and aluminized.

The fibers sit inside grooves between the steel plates as shown in Fig. 1.1b. Each side of a TileCal module is read out by separate fibers leading to separate PMTs, thus leading to a redundancy in case of PMT/electronics failure for a particular channel.

A pseudo-projective readout in η was made possible by the appropriate grouping of WLS fibers to the same PMT.

The total number of fibers needed to read out the whole calorimeter is 640,000 amounting to a total length greater than 1000 km.

To hold the fibers in the groove and against the tile, a special reflective plastic profile was designed which could be easily pressed into the groove between the steel plates as shown in Fig. 1.1b. The fibers directly couple to the edges of the tiles which they are reading out, and are shielded inside the profile when traversing tiles they are not reading out. Only the portion of the fiber directly coupled to the tile needs to be wavelength-shifting and so consideration was given to splicing the WLS portion of the fiber to a clear fiber that would then be routed to the PMT. This would both improve the light yield (clear fiber has a larger attenuation length), as well as reducing Cerenkov and scintillation light produced in the fibers themselves. This is particularly a problem for muons traversing the ϕ crack between modules, creating the potential for large non-uniformities. This problem is reduced by the addition of a small amount of UV absorber to the fibers, and it was decided not to pursue the option of splicing. Fibers and profiles arrived at the construction site as a unit premade by a robotic system for fiber insertion into the profiles.

There is a great deal of flexibility in the manner in which the WLS fibers could be routed to the PMTs. There were a number of considerations that led to the optimal solution:

- the non-uniformities within the cell should be minimized;
- the light output should be maximized;
- the fiber length should be minimized;
- the non-uniformities among cells should be small;
- the number of different fiber lengths should be kept as small as possible;
- sharp bends (radius less than 5 cm) should be avoided in the fiber routing.

A picture of the fiber routing in progress for one of the extended barrel modules is shown in Fig. 1.4b. Above the module fibers is a template used for guidance.

The average light output of a tile is inversely proportional to the area of the tile and linearly proportional to the tile-fiber coupling length. As the PMTs are located at the outer radius of each module, the tiles with the largest area have the shortest fiber path, leading to a better equalization of the light yields from the 11 layers of tiles. The fibers for each cell on each side are combined into a bundle and routed to the respective PMT position. This position is as close to the geometric center of the cell as possible in order to equalize the needed fiber lengths. Each bundle is glued and then the ends polished after the glue hardens. A special cutting/polishing machine was developed that traversed the inside of the girder.

Due to space constraints, the TileCal ITC consists only of scintillators at high η values (1.0-1.6). The gap scintillators cover the η region from 1.0 to 1.2, while the cryostat, or crack, scintillators (located between the central and endcap elec-

10 *K. Anderson², T. Del Prete⁴, E. Fullana¹, J. Huston³, C. Roda⁴ and R. Stanek¹*

tromagnetic calorimeter cryostats) cover the η region from 1.2 to 1.6. The energy deposited in the gap scintillators is used to correct the hadronic energy response, while the cryostat scintillators are crucial for correcting the electromagnetic energy response. As the gap and cryostat scintillators consist of single pieces of scintillator, the highest light yield scintillator from Bicron (BC408) was purchased for their fabrication.

The highest expected radiation dose for the TileCal is approximately 40 Gy/year, at η of 1.2. The cryostat scintillators, given their location, will accumulate approximately 1 kGy/year, which will lead to significant light loss, and thus have been designed for easy replacement/installment.

1.2.6. Readout

The TileCal front-end electronics design allows calibration and monitoring of the readout system to better than 1%.¹⁵ It measures cell energies from 30 MeV to 2 TeV for the 10,000 channels of the front-end readout. The precision and noise levels of the electronics system does not significantly degrade the resolution of the calorimeter energy measurement, which is set by the fluctuations in the physics of the hadronic showers.

1.2.6.1. Mechanics and Overview

The TileCal front-end electronics resides inside the backbone support girders of the calorimeter wedges (See Fig. 1.6). This position has the advantage of low radiation levels, low magnetic field, and places the electronics behind the active elements of the calorimeter where the hadronic showers occur. The electronics is located in an element (drawer) that slides into the girder. Limited space and accessibility make compactness and reliability important design criteria.

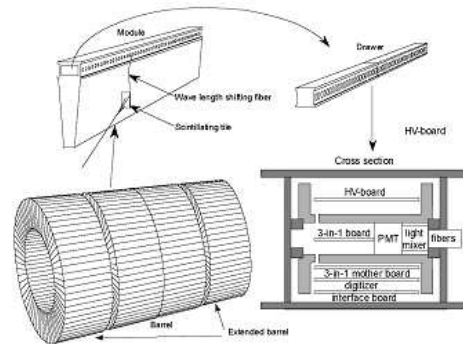


Fig. 1.6. Schematic diagram of the TileCal, its wedge-shaped modules with removable drawers, along with a cross section of a drawer.

The front-end electronics must process the signals generated from the PMTs.

The size of these signals range from a single MIP (e.g. a muon) traversing the detector up to a 2 TeV shower. The latter corresponds to a signal of up to 800 pC from each of the two PMTs associated with a calorimeter cell. The requirement set by the resolution for a MIP and by the dynamic range demands a 16 bit range digitization. This requirement is met by passing the PMT pulse through a shaping stage to remove any shape fluctuations present in the raw PMT signal, amplifying the pulse in two gain scales and then digitizing the resulting signals in 40 MHz 10 bit flash ADC's. Calibration and trigger functions must also be carried out.

The front-end electronics consists of several subsystems:

- (1) the 3-in-1 cards inside the PMT magnetic shielding can;
- (2) the motherboard system which controls up to 48 3-in-1 cards in the drawer and supports tower trigger sum cards and an integrator ADC card;
- (3) digitizer boards;
- (4) the optical interface board.

1.2.6.2. The 3-in-1 card

Figure 1.7 shows a functional diagram of the 3-in-1 card. Most analog functions of the front-end electronics are contained on a 7 cm by 4.7 cm printed circuit board, called the 3-in-1 card, located inside the steel shield of each PMT block.

The shaped PMT signals are produced in a passive LC shaping network. This network removes the pulse to pulse signal shape fluctuation in the raw PMT pulse producing a standard signal shape for all channels of the TileCal system. The extremely low noise of the passive LC shaping network is critical in maintaining the 16 bit dynamic range requirement. The shaped signal is passed to 2 operational amplifiers that produces two signals for high and low gain range. The amplifiers have a gain ratio of 64 and have a clamping design. Clamping amplifiers provide fast recovery from saturation, which is particularly important for the high gain amplifier. The amplified signals are then passed to differential drivers which send the signals to the digitizer boards.

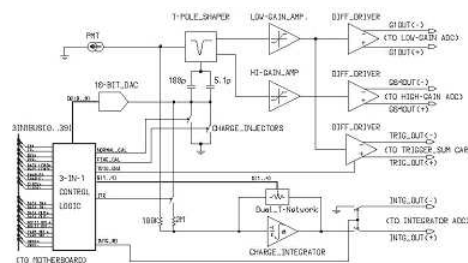


Fig. 1.7. Block diagram of the TileCal 3-in-1 card.

In addition to the high and low gain outputs sent to the digitizer boards, a

12 *K. Anderson², T. Del Prete⁴, E. Fullana¹, J. Huston³, C. Roda⁴ and R. Stanek¹*

differential fast trigger signal, derived from the low gain output is sent to the trigger sum boards mounted on the mother boards in order to produce trigger tower sums. The fine timing requirements for the analog sums are satisfied by using appropriate cable lengths. The outputs of the tower sum boards are sent to the level 1 trigger system.

A charge injection system is designed the whole electronic channel. Two capacitors (5.1 pF and 100 pF) are connected through fast switches to the shaping network. When the switch is closed, a fast pulse is sent through the shaping network. The 100 pF capacitor can calibrate the system over the full 800 pC range, while the small 5.1 pF capacitor calibrates up to about 40pC and giving a finer scale for calibrating the high gain channel.

The PMT signal is also received form the slow integrator amplifier. This amplifier averages over a time period of 10ms the DC level of the PMT signal. This signal is multiplexed onto a bus on the mother board and sent to the Integrator ADC card which contains a microprocessor, ADC, and a CANBUS interface. It digitizes the integrator amplifier signal level and transmits the data to the counting room via CANBUS. These signals are used in the radioactive source calibration of the PMT signals discussed in section ??.

The charge injection must be fast because its phase relative to the digitization clock must be maintained to control the time of digitization relative to the peak amplitude.

1.2.6.3. *Motherboard Control System*

A small ALTERA EPLD on the 3-in-1 card holds the configuration settings sent from the motherboard control system. Most commands are sent serially into the ALTERA chip, but some commands like the charge injection signal are passed directly. Digital control of the 3-in-1 cards is needed for the charge injection calibration, in order to control the gain of the charge integrator, to control the switching of the charge integrator output onto the analog bus, and to enable/disable the trigger summation output. The control signals are supplied by a motherboard which runs the length of the electronics drawer. The TTC system (Trigger, Timing and Control¹⁶) is the primary means of control and must be used for precise timing of charge injection functions. Read back of 3-in-1 card control settings via the CANBUS channel is very useful in accessing the state of the system.

Commands can be sent to individual 3-in-1 cards or broadcast system-wide to all cards armed to receive such commands. This allows the system to be configured in a complex pattern to inject charge based on a Monte Carlo generated event simulation. In broadcast mode, one can quickly step all channels through a calibration procedure.

A more detailed description of the 3-in-1 card and motherboard system can be found here.¹⁷

1.2.6.4. Digitizers

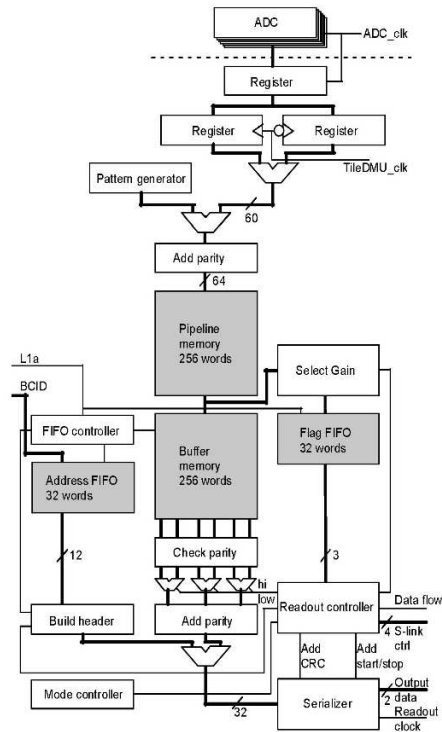


Fig. 1.8. A simplified block diagram of the TileCal digitization system.

A functional diagram of the digitization system is shown in Fig. 1.8. The digitizer boards (8 per drawer) each receive the high and low gain differential signals from six 3-in-1 cards. These signals are digitized every 25 ns by 10-bit ADCs, using a TTC system clock that can be adjusted in units of 106 ps. In this way we can phase correctly the signal to time the ADC sampling time. The TTC system clocks provide precise timing relative to the accelerator time structure. Each ADC has a programmable DC offset to prevent the ADC from receiving negative signals.

The digitized data words are processed by a so-called TileDMU custom ASIC chip which temporarily stores the data in pipeline memories. The pipeline length is programmable up to 256 samples giving a pipeline latency of up to 6.4 μ s, which is considerably longer than the 2.5 μ s ATLAS requirement. The latency is needed to let the level 1 trigger system to make a decision and to return a level 1 accept (L1A) trigger signal to the digitizer system.

At reception of an L1A signal, the TileDMU captures an event frame and sends it to an output storage memory. The position of the event frame along the pipeline and the number of data samples stored are programmable. Typically when running

14 *K. Anderson*², *T. Del Prete*⁴, *E. Fullana*¹, *J. Huston*³, *C. Roda*⁴ and *R. Stanek*¹

at a L1A trigger rate of 100 kHz 7 samples are recorded. The captured event is all at either high or low gain depending on the value of the maximum sample in the event frame. If the maximum sample is below a programmable maximum value in the high gain data, high gain samples are selected. Otherwise, low gain samples are sent to memory. Overlapping event frames are permitted and L1A trigger signals can be processed with a three bunch crossing (75ns) separation.

With each event frame data block, a header word is stored in memory. This header word contains the bunch crossing identification number of the event, various diagnostic flags (e.g., parity words) and the gain scale flag bit.

The output memory can buffer 36 events at 7 samples. A control process monitors the output memory and sends events serially to the Optical Interface Card along with control signals and the data clock.

A more detailed description of the digitization system can be found elsewhere.¹⁸

1.2.6.5. *Optical Interface Card*

The optical interface card receives the serial data streams from the 16 TileDMU chips in the drawer. It realigns the data to a common clock and packs it into 32 bit words and transmits data over optical links to the readout driver (ROD) crates in the counting room. Cyclic redundancy checks are performed on the data link between the digitizers and the interface card and between the interface cards and the RODs. The interface card memory holds 16 events at 7 samples.

1.2.7. *The monitoring system*

TileCal is complemented by four systems to monitor, test and calibrate the calorimeter readout at various stages. The use of four systems provides a reasonable redundancy to both control and monitor the performances and the overall calibration. Moreover the calibration systems have been heavily used during the instrumentation and commissioning of the TileCal, especially to check and eventually repair any defective channels.

1.2.7.1. *The Charge Injection System*

The linearity and stability of the front end electronics, and the stability of the two gain circuits, are monitored by injecting a precise charge at the input stage of each electronic channel. With this method we can precisely calibrate the readout of each ADC channel from ADC counts to pC.

1.2.7.2. *The Radioactive ¹³⁷Cs System*

The final calibration of the calorimeter at the electromagnetic scale can only be performed using electron beams of known energy. Given the complexity of the

detector only the external cells can be directly calibrated with electrons. The calibration is transported to the inner cells with high precision using the Cs system. In this system the TileCal optics is monitored by exciting each scintillating tile with a moving radioactive source. Through this technique, we can monitor and equalize the scintillator light yield, the scintillator coupling to the WLS fibers and the integrity of these fibers to transport light to the PMT. TileCal is equipped with three calibrated ^{137}Cs sources - one for the barrel and one for each of the extended barrels. The sources travel in tubes passing through each scintillator tile, their motion controlled by a hydraulic fluid. The DC current from each PMT is measured by the integrator system described above. In this manner, an x-ray picture of the detector is obtained^{19,20}. Equalization is obtained by adjusting the voltage of each PMT. The resulting inter-module calibration is consistent within a few per mil. Fig. 1.9 shows the working principle of the system and an example of the analysis of Cs data taken during the calorimeter commissioning. The accuracy in measuring the single tile response is about 2%.

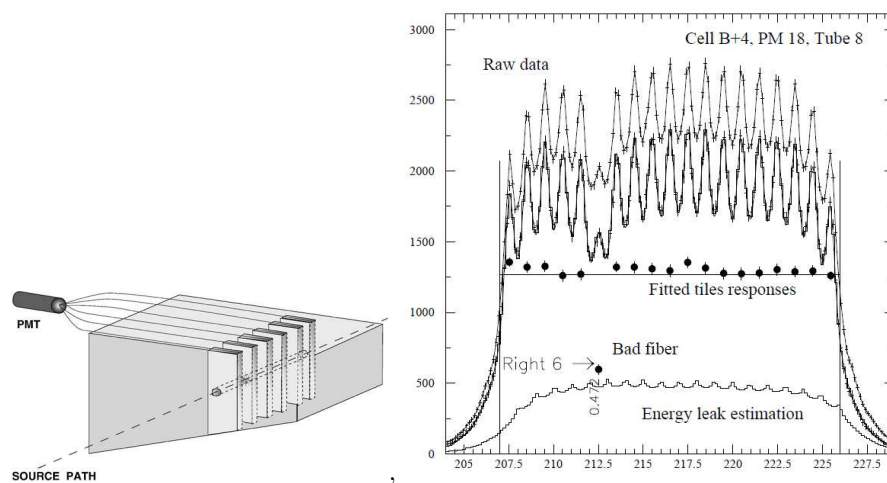


Fig. 1.9. (a) The Cesium source monitoring concept. (b) An example of calibration data analysis taken during Tile Commissioning; one tile to fiber coupling was found to be defective and afterwards was fixed.

1.2.7.3. The laser system

The PMT performances and the fast readout chain is monitored with fast laser light pulses transported to the photocathode of each PMT by dedicated clear, plastic optical fibers. The shape of the laser signal is very similar to that of the scintillating light and its amplitude covers the whole dynamic range up to the saturation level of the PMTs. The PMT gain, stability and their linearity can be monitored at a

16 *K. Anderson*², *T. Del Prete*⁴, *E. Fullana*¹, *J. Huston*³, *C. Roda*⁴ and *R. Stanek*¹

level better than 1%.

1.2.7.4. *The Minimum Bias Current System*

The slow integrator system will monitor, during LHC stable beam operation, the current in each PMT due to Minimum Bias events. The integration time is set to 10 ms with different amplifications to cope with the large dynamic range needed.

1.3. Performance of the Tile Calorimeter

The main requirements that drove the TileCal design were performance on energy measurement and practical considerations such as cost and the need for an easy construction. While the latter two issues have been addressed in the previous sections, in this section the performance requirements are considered in more detail.

The key variables needed to evaluate the calorimeter performance are energy linearity and resolution. TileCal is required to have a maximum deviation from linearity of a few percent for energy deposit ranging from a few hundreds of MeV, corresponding to muons passing through the calorimeter, up to a few TeV. The linearity requirement has an impact on basically all jet measurements and it is particularly important for the sensitivity to new physics. As an example, a deviation of few percent from linearity would mask a signal of compositeness at the scale of 20-30 TeV.[?]

The energy resolution is required to be of the order of $50\% \sqrt{E(\text{GeV})} \oplus 3\%$. This would give a mass resolution better than 10% for decays $W \rightarrow jj$. Clearly, the quoted global performances on the jet energy measurement are defined by the characteristics of both the electromagnetic and hadronic sections of the calorimeter.

TileCal is based on a semi-projective geometry where each tower is segmented in three longitudinal layers. While the transverse cell dimension is determined to be of the order of the hadronic shower lateral spread ($\lambda \simeq 23 \text{ cm}$), the longitudinal cell dimension varies layer by layer. Various choices have been considered for the longitudinal dimension of the layers, the final design consists of two relatively thin layers interleaved by a thick central layer. The width of the first longitudinal layer is chosen to be sensitive to the energy losses in the passive material lying between the electromagnetic and the hadronic calorimeter sections. In fact the correlation between this energy deposit and the one in the last electromagnetic calorimeter layer is used to correct for the energy losses in the passive material. The width of the central layer is large enough to sample the bulk of the shower while the last layer acts as a kind of tail catcher.

The length of each longitudinal layer is large enough to provide an integrated muon signal that could be well separated from noise, and used to form an alternative source for a muon trigger. This could be particularly useful for the low energy muons that do not reach the outer layers of the muon spectrometer.

At $\eta = 0$ the total length of the instrumented region is about 8.2λ including

the 1.2λ of the three electromagnetic sections and the $1.4, 4$ and 1.8λ of the three TileCal sections.

The longitudinal segmentation of the LAr and TileCal sections is very important to obtain information on the shower shape and therefore on the shower composition. In fact, since both calorimeter sections are non-compensating, the shower shape information is used to implement software techniques to correct the calorimeter response. This procedure is essential to be able to meet both the linearity and resolution requirements on the energy measurement of hadronic showers.

1.3.1. Measuring the Performance with Test Beams

The first TileCal R&D program dates back to 1991, and the final module construction started in 1998. The modular construction has allowed, during the construction years, to carry out various tests in beams on a total of about 12% of the calorimeter modules. The primary aim of these tests was to calibrate the energy scale of the calorimeter.²¹ These measurements have also been very important to improve the GEANT4²² description of hadronic showers in the TileCal.

The modules in the testbeam were placed on a moveable table, which allowed the beam to be directed to any point of the outer perimeter. The cell-by-cell response was then equalized using the Cesium source resulting in a uniformity of the order of few per mil. During the equalization procedure, the PMT voltages are adjusted to measure about 1.1 pC/GeV for electrons. The value chosen for the signal equalization is determined by the need to measure, with the highest precision, both the low and the high end of the dynamic range.

The precise measurement of the electromagnetic calibration constant is then obtained using electron beams of momentum ranging between 20 and 180 GeV/c, directed at 20 degrees on all the cells of the first calorimeter layer (A cells). The energy deposit is almost completely contained in a single cell. The cell-by-cell calibration uniformity, evaluated by the RMS of the calibration constants of all the calibrated cells, is $2.4 \pm 0.1\%$ (Fig. 1.10 (a)). This residual spread is due to local variation in individual tile and tile/fiber responses as confirmed by MonteCarlo studies.²³

The electron beam used to calibrate the outer cells of the modules does not give any information on the inner cells. The uniformity of the response of the inner cells is therefore verified with muon beams. Figure 1.10(b) shows the mean response to 180 GeV/c muons, normalized to the path length, as a function of the pseudorapidity (full circles). The calibration uniformity over the whole η range (averaged on different longitudinal layers) is less than 1%.

The overall performance of the calorimeter is measured with pions. During the test beam studies, a large data sample of pions with momentum ranging from 20 to 180 GeV/c has been acquired. Figure 1.11 shows the energy linearity and resolution, at the electromagnetic scale, for pions impinging on the calorimeter at $\eta = 0.35$ for

18 *K. Anderson², T. Del Prete⁴, E. Fullana¹, J. Huston³, C. Roda⁴ and R. Stanek¹*

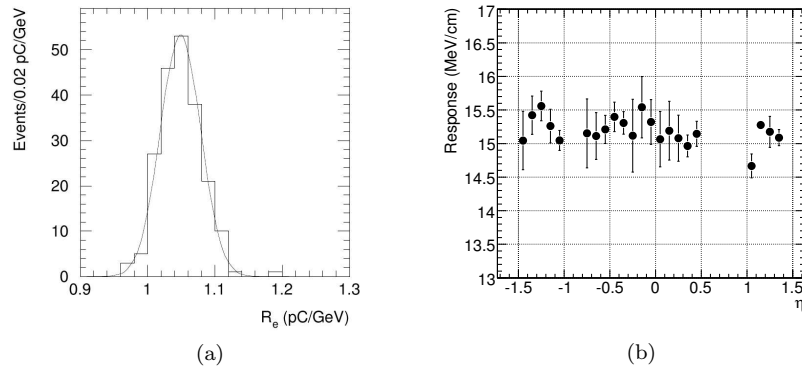


Fig. 1.10. (a) The cell response of electrons entering the calorimeter modules exposed to the beam at incidence angle of 20 degrees, normalized to beam energy, with one entry for each A-cell measured. The plot contains data at various energies ranging from 20 to 180 GeV. The mean value, 1.050 ± 0.003 pC/GeV, defines the TileCal electromagnetic scale factor. The RMS spread is (2.40.1)%. (b) The total calorimeter response to 180 GeV muons, normalized to the path length, as a function of pseudorapidity.

data (full circles) and Geant4^a simulation (open squares). Since the plots are shown at the electromagnetic scale the non-compensation effects are clearly visible on the linearity plot. The Geant4 simulation describes both the linearity and resolution within a few percent over the whole energy range.

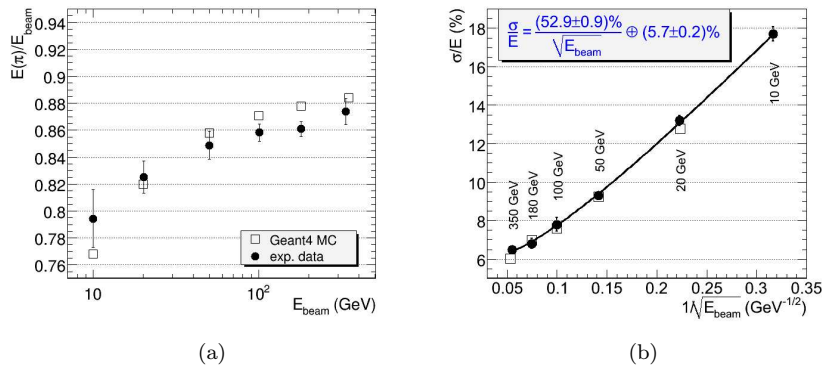


Fig. 1.11. Energy linearity (a) and resolution (b) at the electromagnetic scale, for pions impinging the calorimeter at $\eta = 0.35$. Both plots show experimental data (full circles) and Geant4 simulated data (open circles).

^aGeant4 version is 4.8.3 and the hadronic list is the QGSP Bertini model.

1.3.2. Experience with the Installed Detector: Cosmic Muons and Single Beam Events

The assembly in the cavern was completed in December 2005 and the TileCal was the first ATLAS sub-detector to provide cosmic muon data. The installation of all the other sub-detectors has been completed and the whole ATLAS detector has been available for cosmic data taking for some time. An example of the events acquired with cosmic muons is given in the event display shown on Fig. 1.12.

Fig. 1.12. Event display of the signal produced by a cosmic muons crossing the central region of the ATLAS detector. Both the solenoid and toroid fields were on during this run.

Once the detector installation phase was completed, the work has concentrated on improving the stability of the whole system and on developing a data quality framework that allowed to quickly identify any problematic channels. Such a system should be automated as much as possible, in order to allow quick diagnostics on 10.000 channels. Data generated with random triggers, with the integrated TileCal control/calibration systems and with cosmic muons have been used both for diagnostic and for stability studies. As an example, the noise stability evaluated on randomly triggered events as a function of time for a period of three months is shown in Figure 1.13 (a). The electronic noise is evaluated by the RMS of the digital samples and is averaged over the whole calorimeter. The relative variation in time is within 1% (represented by the green dotted lines) and the average value is 1.44 ADC counts. The time dependence of the electronic noise for a single typical channel is also shown.

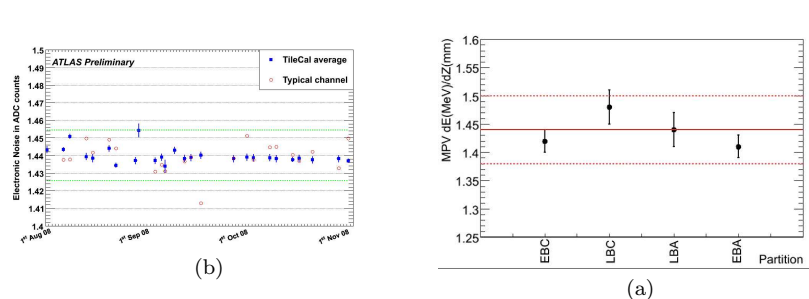


Fig. 1.13. (a) Time dependence of the electronic noise stability evaluated, on randomly triggered events, by the RMS of the digital samples averaged over the whole calorimeter. The green dotted lines represent the $\pm 1\%$ variation from the average values (b) Most Probable Value of dE/dx signals recorded by TileCal with horizontal muons from single beam data on Sept. 10, 2008. The average response over all cells within a given partition to horizontal muons is shown for each partition. About 500 muons were selected by requiring a consistency to the expected signal along 12 m of Tile calorimeter length. This data provided the opportunity to verify the intercalibration of the TileCal cylinders, already calibrated with radioactive gamma sources, down to the 4% precision level. The red lines represent the average MPV value of the 4 barrels and its 4% uncertainty.

20 *K. Anderson*², *T. Del Prete*⁴, *E. Fullana*¹, *J. Huston*³, *C. Roda*⁴ and *R. Stanek*¹

On September 10, 2008, LHC had started to operate and single proton beams were successfully circulated in both directions. The interaction of these beam with collimators, lying 148 meters upstream of the ATLAS detector, produced the so called "splash" events. In these events, the many particles produced in the beam interaction with the collimator reached the ATLAS detector producing signals in all the sub-detectors. These events allowed us to carry out the first studies of TileCal performance with beam-generated particles.²⁴ The muons that traverse the TileCal horizontally provide useful information on inter-calibration of the three barrels. Figure 1.13 (a) shows the Most Probable Value of dE/dx signals recorded by TileCal when traversed by horizontal muons. Each point in the plots shows the average value calculated over all cells within a given barrel (the central barrel is divided in two parts). The barrel to barrel inter-calibration is within 4%.

References

1. O. Gildemeister, F. Nessi-Tedaldi, and M. Nessi, An Economic Concept for a Barrel Hadron Calorimeter with Iron Scintillator Sampling and WLS-Fiber Readout. Prepared for 2nd International Conference on Calorimetry in High-energy Physics, Capri, Italy, 14-18 Oct 1991.
2. M. Bosman et al., Developments for a Scintillator Tile Sampling Hadron Calorimeter with Longitudinal Tile Configuration: R & D Proposal. CERN-DRDC-93-3.
3. F. Ariztizabal et al., Construction and Performance of an Iron Scintillator Hadron Calorimeter with Longitudinal Tile Configuration, *Nucl. Instrum. Meth.* **A349**, 384–397, (1994). doi: 10.1016/0168-9002(94)91201-7.
4. P. Jenni, P. Sonderegger, H. P. Paar, and R. Wigmans, The High Resolution Spaghetti Hadron Calorimeter: Proposal. NIKHEF-H/87-7.
5. V. Semenov. Proc. of the IX Conference on Scintillators, Kharkov. 1986, pag 86.
6. M. Kadykov. Preprint JINR 13-90-10. Dubna, 1990.
7. J. Abdallah et al. The Production and Qualification of Scintillator Tiles for the ATLAS Hadronic Calorimeter. Technical Report ATL-TILECAL-PUB-2007-010. ATL-COM-TILECAL-2007-026, CERN, Geneva (Dec, 2007). This note written by IHEP Group, Protvino.
8. M. David, A. Gomes, A. Maio, J. Pina, and B. Tom. 15 Years of Experience with Quality Control of WLS Fibers for the ATLAS Tile Calorimeter. Technical Report ATL-TILECAL-PUB-2008-003. ATL-COM-TILECAL-2007-022, CERN, Geneva (Dec, 2007).
9. M. David, A. Gomes, and A. Maio. Radiation Hardness of WLS Fibers for the ATLAS Tile Calorimeter. Technical Report ATL-TILECAL-PUB-2008-002. ATL-COM-TILECAL-2007-021, CERN, Geneva (Dec, 2007).
10. F. Bosi, S. Burdin, V. Cavasinni, D. Costanzo, T. D. Prete, V. Flaminio, E. Mazzoni, C. Roda, G. Usai, and A. Vasiljev, A Device to Characterize Optical Fibers, *Nuclear Instruments and Methods in Physics Research Section A: Accelerators, Spectrometers, Detectors and Associated Equipment*. **485**(3), 311 – 321, (2002). ISSN 0168-9002. doi: DOI:10.1016/S0168-9002(01)02067-8. URL <http://www.sciencedirect.com/science/article/B6TJM-44CXYSS-9/2/9d17476b%1b7b60a95c21b163c2eee68a>.
11. ATLAS Tile Calorimeter: Technical Design Report. CERN-LHCC-96-42.
12. ATLAS: Detector and Physics Performance Technical Design Report. Vol. 1. CERN-

- LHCC-99-14.
13. ATLAS: Detector and Physics Performance Technical Design Report. Vol. 2. CERN-LHCC-99-15.
 14. B. A. Alikov et al., ATLAS Barrel Hadron Calorimeter: General Manufacturing Concepts for 300 000 Absorber Plates Mass Production. JINR-E13-98-135.
 15. K. Anderson et al. ATLAS Tile Calorimeter Electronics. <http://hep.uchicago.edu/atlas/tilecal>.
 16. M. Ashton et al., Timing, Trigger and Control Systems for LHC Detectors. CERN-LHCC-2000-002.
 17. K. Anderson et al., Design of the Front-End Analog Electronics for the ATLAS Tile Calorimeter, *Nucl. Instrum. Meth.* **A551**, 469–476, (2005). doi: 10.1016/j.nima.2005.06.048.
 18. S. Berglund et al., The ATLAS Tile Calorimeter Digitizer, *JINST.* **3**, P01004, (2008). doi: 10.1088/1748-0221/3/01/P01004.
 19. E. Starchenko et al., Cesium Monitoring System for ATLAS Tile Hadron Calorimeter, *Nucl. Instrum. Meth.* **A494**, 381–384, (2002). doi: 10.1016/S0168-9002(02)01507-3.
 20. N. Shalanda et al., Radioactive Source Control and Electronics for the ATLAS Tile Calorimeter Cesium Calibration System, *Nucl. Instrum. Meth.* **A508**, 276–286, (2003). doi: 10.1016/S0168-9002(03)01700-5.
 21. K. J. Anderson et al., Calibration of ATLAS Tile Calorimeter at the Electromagnetic Scale. (2009). ATL-TILECAL-PUB-2009-002.
 22. J. Allison et al., Geant4 Developments and Applications, *IEEE Trans. Nucl. Sci.* **53**, 270, (2006). doi: 10.1109/TNS.2006.869826.
 23. T. Davidek et al., Testbeam Studies of Production Modules of the ATLAS Tile Calorimeter. (2009). To be published in NIM A.
 24. H. Okawa, Commissioning of the ATLAS Tile Calorimeter with Cosmic Ray and Single Beam Data. ATL-TILECAL-PROC-2008-002.